Roxane E. Vella,[1,2,3] Nicolas J. Pillon,[1,2,3] Bader Zarrouki,[1,2,3] Marine L. Croze,[1,2,3] Laetitia Koppe,[1,2,3] Michel Guichardant,[1,2,3] Sandra Pesenti,[1,2] Marie-Agnès Chauvin,[1,2] Jennifer Rieusset,[1,2] Alain Géloën,[1,2,3] and Christophe O. Soulage[1,2,3]

Ozone Exposure Triggers Insulin Resistance Through Muscle c-Jun N-Terminal Kinase Activation

Diabetes 2015;64:1011–1024 | DOI: 10.2337/db13-1181

A growing body of evidence suggests that exposure to traffic-related air pollution is a risk factor for type 2 diabetes. Ozone, a major photochemical pollutant in urban areas, is negatively associated with fasting glucose and insulin levels, but most aspects of this association remain to be elucidated. Using an environmentally realistic concentration (0.8 parts per million), we demonstrated that exposure of rats to ozone induced whole-body insulin resistance and oxidative stress, with associated endoplasmic reticulum (ER) stress, c-Jun N-terminal kinase (JNK) activation, and disruption of insulin signaling in skeletal muscle. Bronchoalveolar lavage fluids from ozone-treated rats reproduced this effect in C2C12 myotubes, suggesting that toxic lung mediators were responsible for the phenotype. Pretreatment with the chemical chaperone 4-phenylbutyric acid, the JNK inhibitor SP600125, or the antioxidant N-acetylcysteine alleviated insulin resistance, demonstrating that ozone sequentially triggered oxidative stress, ER stress, and JNK activation to impair insulin signaling in muscle. This study is the first to report that ozone plays a causative role in the development of insulin resistance, suggesting that it could boost the development of diabetes. We therefore provide a potential mechanism linking pollutant exposure and the increased incidence of metabolic diseases.

Type 2 diabetes (T2D) is one of the most prevalent metabolic diseases worldwide and is projected to increase dramatically over the next decades because of aging populations, chronic overnutrition, and sedentary lifestyle. Environmental and lifestyle-related factors can account for roughly 90% of adult-onset diabetes (1), and it has been suggested that T2D can be prevented by lifestyle and diet modifications (2). There is also growing evidence for an association between traffic-related air pollution and the incidence of T2D. For instance, the hazards for diabetes were increased with particulate matter (PM) exposure (3), whereas a statistically significant association of nitrogen dioxide (NO_2) was detected with confirmed cases of diabetes or with mortality from diabetes (4,5). In advanced polluted air environments, the action of ultraviolet (UV) rays on volatile organic compounds or NO_2 is responsible for the formation of ozone (O_3), another major pollutant in urban areas (6). O_3 pollution has become a major environmental challenge because of large exposed human populations both in the Western world and in developing countries (7). Children and the elderly are particularly sensitive to the pulmonary health effects of O_3, inducing or worsening asthma, chronic obstructive pulmonary diseases, and lung inflammation (8,9). In addition, many extrapulmonary effects of O_3 have been described: activation of stress-responsive regions, catecholamine biosynthesis, cell degeneration, neurochemical alterations in the central nervous system (10,11), increased production of nitric oxide, enhanced protein synthesis and inflammation in the liver (12), compensatory changes, edema,

[1]Université de Lyon, Oullins, France
[2]Institut National de la Santé et de la Recherche Médicale, UMR 1060 CarMeN, Laboratoire de Recherche en Cardiovasculaire, Métabolisme, Diabétologie et Nutrition, Villeurbanne, France
[3]Institut National des Sciences Appliquées de Lyon, Multi-disciplinary Institute of Lipid Biochemistry (IMBL), Villeurbanne, France
Corresponding author: Christophe O. Soulage, christophe.soulage@insa-lyon.fr.

Received 31 July 2013 and accepted 27 September 2014.

This article contains Supplementary Data online at http://diabetes.diabetesjournals.org/lookup/suppl/doi:10.2337/db13-1181/-/DC1.

R.E.V. and N.J.P. contributed equally to this work.

A.G. and C.O.S. contributed equally to this work.

See accompanying article, p. 712.

and increased oxidative stress in heart tissue (13,14). Taken together, these studies demonstrate that O_3 can exert many deleterious effects in distant tissues.

The role of oxidative stress in the etiology and pathogenesis of human diseases has been widely described in the past 2 decades (15). Many studies pinpoint oxidative stress as a potential cause to both the onset and progression of T2D (16–18) and its associated complications, such as endothelial dysfunction and cardiovascular diseases (19,20). O_3 is a strong oxidant, and, although not a radical species, most of its toxic effects are mediated through free radical reactions (21,22). Oxidative stress is indeed implicated in many deleterious effects of O_3, such as pulmonary inflammation and dysfunction (23), Alzheimer's disease (24), and cardiovascular diseases (25). In a recent study, Bass et al. (26) demonstrated that O_3 impaired glucose homeostasis in rats; however, very little is known about the effects of O_3 on metabolism and metabolic diseases.

Despite being a key issue for public health, the putative role of O_3 exposure in the onset and progression of diabetes remains poorly defined. Our study demonstrates for the first time that exposure to O_3, at a concentration realistically mimicking human exposure, induces insulin resistance (IR) in rodents, therefore suggesting a significant contribution of O_3 in the etiology of T2D.

RESEARCH DESIGN AND METHODS

Chemicals, Reagents, and Antibodies

All chemicals and culture media were purchased from Sigma-Aldrich (Saint Quentin Fallavier, France) when no other origin is specified. Recombinant human insulin (100 IU/mL; Actrapid) was from Novo Nordisk (La Défense, France). Anti-phospho-Akt 1/2/3 rabbit IgG (catalog #7985R) and anti-Akt 1/2/3 rabbit IgG (catalog #8312) antibodies were purchased from Santa Cruz Biotechnology (Heidelberg, Germany), anti-tubulin mouse IgG antibody was from Sigma-Aldrich, and anti-mouse IgG and anti-rabbit IgG antibodies were from Bio-Rad (Marnes-la-Coquette, France). Endoplasmic reticulum (ER) stress antibodies were all included in the ER Stress Antibody Sampler Kit from Cell Signaling Technology (Saint-Aubin, France). Super Signal West Pico Chemiluminescent Substrate and Restore Western Blot Stripping Buffer were obtained from Thermo Scientific (distributed by Perbio Sciences France, Brebières, France).

Animal Care

Animal experiments were performed under authorization 69–266–0501 (INSA-Lyon, Direction Départementale de la Protection des Populations-Services Vétérinaires du Rhône), according to the ethical guidelines laid down by the French Ministère de l'Agriculture (87–848) and the European Union Council Directive for the Care and Use of Laboratory Animals of November 24th, 1986 (86/609/EEC). Authors A.G. (license 69266332) and C.O.S. (license 69266257) hold special licenses to experiment on living vertebrates that were issued by the French Ministry of Agriculture and Veterinary Service Department. Wistar rats weighing 400–450 g (Janvier SA, Le Genest-Saint-Isle, France) were housed in an air-conditioned room at 24 ± 1°C with a 12-h light/dark cycle (light on at 6:30 A.M.) with free access to food (13.4 kJ/g, 65% carbohydrates, 11% fat, 24% proteins, weight for weight; diet A03; SAFE, Augy, France) and water. Great care was taken to minimize animal discomfort and suffering during the experimental protocol.

O_3 Exposure

Rats were kept within a Plexiglas hermetic environmental chamber (width 0.35 m, length 0.70 m, height 0.40 m, surface 0.25 m^2, volume 0.1 m^3) supplied with a constant airflow (6 m^3/h) and subjected to 1,570 $\mu g/m^3$ O_3, corresponding to 0.8 parts per million (ppm) for 16 h, as previously described (10). O_3 was generated by passing filtered air across a UV light, and concentration inside the cage was controlled by adjusting the inlet flow of air. The O_3 concentration was continuously measured using a calibrated UV photometric O_3 monitor (range ± 0.001 ppm; catalog #41M; Environement SA, Poissy, France) connected to the outlet line of the chamber. Control exposure was performed in a similar chamber provided with filtered room air at the same flow rate. All the exposures were performed during the dark phase (i.e., the active phase for the rats). Rats were fasted during the exposure but had free access to water. The temperature and relative humidity measured in the chambers during the exposure were 25.3 ± 0.4°C and 75%, respectively. Ammonia and CO_2 concentrations remained undetectable. The mean O_3 concentration inside the exposure chamber was 0.800 ± 0.05 ppm. Of note, the O_3 concentration in the control chamber remained undetectable (<0.001 ppm). Rats were exposed during nighttime, namely, during their active phase, because O_3 pollution peaks generally take place during the day (i.e., during human active phase).

Pretreatment with N-Acetylcysteine or 4-Phenylbutyric Acid

Some rats were pretreated for 10 days with N-acetylcysteine (NAC) prior to O_3 exposure. Rats were given NAC orally in drinking water (10 mmol/L). The water intake was monitored daily to calculate the daily NAC intake. The mean daily intake of NAC was 225 ± 10 mg/kg/day. Another independent set of rats was gavaged daily with 4-phenylbutyric acid (PBA; 150 mg/kg) for 4 days prior to O_3 exposure.

Euglycemic-Hyperinsulinemic Clamps

Euglycemic-hyperinsulinemic (EH) clamps were performed essentially as previously described (27). In brief, Wistar rats were implanted with indwelling catheters in the left carotid artery and right jugular vein. The rats were allowed to recover from the surgery for 5 days. Prior to the EH clamp, the rats were fasted overnight and a standard 2-h EH clamp was conducted using a primed and continuous infusion of human insulin at a rate of 6 mU/kg/min coupled with a variable infusion of 25% (weight for volume) glucose to maintain blood glucose concentrations

at ~6 mmol/L. The glucose infusion rate (GIR) was calculated as the amount of glucose perfused to maintain euglycemia during the second hour of the clamp and was expressed as milligrams of glucose per kilogram per minute.

Insulin Secretion Test With L-Arginine

After an overnight fast, Wistar rats with indwelling catheters were injected intravenously with 1 g/kg L-arginine in saline solution. Blood was withdrawn from an arterial catheter and centrifuged (1 min, 3,500*g*), and plasma samples were snap frozen in liquid nitrogen and stored at −20°C until insulin assay.

Insulin Tolerance Test

After overnight fast, animals were injected intraperitoneally with 0.50 IU/kg body wt recombinant human insulin. Blood glucose was measured before, and 15, 30, 60, 90, and 120 min after insulin injection. Blood glucose values were determined from a drop of blood sampled from the terminal portion of the tail using a glucometer. As previously described (28), the glucose disappearance rate for an insulin tolerance test (ITT) (K_{ITT}; reported as the percentage per minute) was calculated as follows: $K_{ITT} = 0.693 \times 100/t_{1/2}$, where $t_{1/2}$ was the half-life calculated from the slope of the plasma glucose concentration, considering an exponential decrement of glucose concentration during the 30 min after insulin administration.

Bronchoalveolar Lavage Fluid

Rats were anesthetized with sodium pentobarbital (35 mg/kg), and a PE-240 tracheal catheter was inserted into the trachea. Bronchoalveolar lavages were performed twice with 1 mL of sterilized Dulbecco's PBS. An aliquot fraction of bronchoalveolar lavage fluid (BALF) was removed for cellular numeration and leukocyte count while the BALF was centrifuged (8,000*g*, 2 min, 4°C) to pellet cells. Supernatants were removed and kept at −80°C. Total proteins in the BALF were determined by the Bradford protein assay. Lipid peroxidation was measured spectrophotometrically by the thiobarbituric acid method (29) using 1.1.3.3-tetramethoxipropane as the standard. Cells were stained by the May-Grünwald Giemsa method for leukocyte counts, and 500 leukocytes were randomly counted in a Malassez cell under an optical microscope (original magnification ×100).

Sacrifice and Tissue Dissection

To study insulin signaling in skeletal muscle, liver, or adipose tissue, rats were injected with insulin (Actrapid 0.75 IU/kg i.p.) or saline solution at the end of O_3 exposure. Thirty minutes after insulin injection, rats were deeply anesthetized with sodium pentobarbital (60 mg/kg i.p.). Lungs, gastrocnemius or tibialis muscles, retroperitoneal white adipose tissue, and liver were rapidly dissected out, snap frozen in liquid nitrogen, and stored at −80°C.

Biochemical Measurements

Plasma total cholesterol, triacylglycerol, and nonesterified fatty acid (NEFA) levels were measured with commercial kits Cholesterol RTU (bioMérieux, Marcy-l'Etoile, France), Triglyceride PAP (bioMérieux), and NEFA-C (WAKO). Levels of plasma insulin (SPIBio, Montigny-le-Bretonneux, France), corticosterone (Cayman Chemicals), tumor necrosis factor-α, and interleukin-1β (eBioscience, Paris, France) were determined with enzyme immunoassays according to manufacturer's recommendations. Plasma aldehydes (i.e., 4-hydroxy-2-nonenal [HNE] and 4-hydroxy-2-hexenal [HHE]) were measured using gas chromatography–mass spectrometry as previously described (30). Plasma malondialdehyde (MDA), reduced glutathione (GSH), and oxidized glutathione (GSSG) levels were measured by high-performance liquid chromatography coupled to fluorescence detection. Carbonyl groups on proteins were determined using 2.4-dinitrophenylhydrazine as described previously (31).

Analysis of Gene Expression in Muscle by Quantitative PCR

Total RNAs from gastrocnemius muscle samples (80–100 mg) were extracted using TRI Reagent (Sigma-Aldrich). Total RNA quantities and qualities were assessed using the Model 2100 Bioanalyzer and RNA 6000 LabChip Kit (Agilent Technologies, Massy, France). Reverse Transcriptions (RNAse H, Takara enzyme) were performed on 1 μg of total RNA. Real-time PCR assays for ER stress genes (Grp78/Bip, Atf4, Atf6, Ire1-α, Perk, total and unspliced Xbp1, and Eif2) were performed using a Rotor-GeneTM 6000 (QIAGEN). Values were normalized to TBP gene expression. The full list of genes and corresponding primer sequences is shown in Supplementary Table 1.

Cell Culture

C2C12 myoblasts (*Mus musculus*) (catalog #CRL-1772; ATCC, LGC Standards, Molsheim, France) were grown and differentiated to myotubes as described previously (28). C2C12 myoblasts were cultured in DMEM supplemented with 10% heat-inactivated FBS (South America Origin; Biowest), 2 mmol/L L-glutamine, 100 units/mL penicillin, and 100 μg/mL streptomycin. When reaching 90% confluence, differentiation was induced by shifting to DMEM supplemented with 2% heat-inactivated horse serum (South America Origin; Biowest). Experiments were performed when >80% of cells had formed myotubes. Cells were serum starved for 2 h prior to the experiments. Cells were incubated for 30 min with 10% (volume for volume [v/v]) BALF diluted in cell culture media (either from O_3 or from control rats). The cell culture medium containing 10% (v/v) BALF was discarded, and cells were further incubated in a fresh medium containing 100 nmol/L insulin for 20 min. Then, cell culture medium was discarded and cells were frozen. LBA cytotoxicity was determined measuring cell viability with an MTT assay (Roche).

Pretreatment for 1 h with the c-Jun N-terminal kinase (JNK) inhibitor SP600125 (10 μmol/L) or PBA (10 mmol/L) was performed prior to BALF incubation. An UltraLinkHydrazide Resin (Thermo Scientific, Illkirch, France) was used as an affinity support for immobilizing

reactive lipid aldehydes present in BALF. C2C12 myotubes were incubated with 10% (v/v) of aldehyde-depleted BALF, as described above.

2-Deoxyglucose Uptake

C2C12 myotubes were incubated for 20 min with 100 nmol/L insulin. Glucose uptake was measured using 2-deoxy-D-[^{3}H]-glucose (747 GBq/mmol; PerkinElmer, Courtaboeuf, France), as described previously (28,32).

Protein Isolation, Immunoprecipitation, and Immunoblotting

Muscle tissue and C2C12 cells were lysed on ice in Standard Lysis Buffer (20 mmol/L Tris, 138 mmol/L NaCl, 2.7 mmol/L KCl, 1 mmol/L MgCl2, 5% glycerol, and 1% NP40, supplemented extemporaneously with 5 mmol/L EDTA, 1 mmol/L Na3VO4, 20 mmol/L NaF, 1 mmol/L dithiothreitol, and a protease inhibitor cocktail) and centrifuged (13,000*g*, 15 min, 4°C). Protein concentration was determined with a Bradford protein assay. Sixty micrograms of protein lysate from skeletal muscle or 30 μg protein lysate from C2C12 cells were separated on SDS-polyacrylamide gels (10%) after heat denaturation (95°C, 5 min) and then transferred onto a nitrocellulose membrane (Hybond-ECL; GE Healthcare, Meylan, France). After transfer, the membranes were blocked with 5% BSA in Tris-buffered saline with Tween for 2 h. Blots were probed overnight with specific primary antibodies at 4°C followed by 1-h incubation at room temperature with secondary antibodies. Protein bands were detected with an enhanced chemiluminescence substrate kit (SuperSignal West Pico; Perbio Sciences France) using an Image Master VDS-CL camera (Amersham Pharmacia, Orsay, France) and quantified by Quantity One (Bio-Rad) or open-source ImageJ (http://rsbweb.nih.gov/ij/index.html) software. Protein phosphorylation levels were normalized to the matching densitometric values of total proteins. Results were expressed as arbitrary units (a.u.).

Data Analysis

Data are expressed as the mean ± SEM. All data were analyzed using GraphPad Prism version 5.0 software (GraphPad Software, La Jolla, CA). Multiple comparisons were performed using ANOVA followed, when appropriate, by post hoc Fisher protected least significant differences tests. The results of ITTs, arginine tests, and clamps were compared by two-way ANOVA (time and treatment). Simple comparisons were performed using the Student *t* test. When appropriate, Welch correction for inequality of variances was applied. Differences were considered significant at the $P < 0.05$ level.

RESULTS

O_3 Exposure Induces IR Through Disruption of Insulin Signaling Pathways in Skeletal Muscle

O_3-exposed rats exhibited a significant rise in fasting blood glucose and insulin concentrations (+23% [$P < 0.01$] and +128% [$P < 0.05$], respectively), while plasma lipid concentrations remained unaltered. Consequently, the HOMA-IR was higher after O_3 exposure (+150%, $P < 0.05$), suggesting an impairment in insulin sensitivity (Table 1). GIR measured using EH clamps (Fig. 1*A* and *B*) was significantly decreased in O_3-exposed rats compared with control rats (9.9 ± 1.9 vs. 24.2 ± 2.1 mg · kg^{-1} · min^{-1}, $P < 0.01$), indicating marked whole-body IR. This was not due to a decrease in insulin secretion capacity, as the acute insulin secretion induced by the nonglucose secretagogue arginine was similar in the two groups (Fig. 1*C*). In good agreement, the results of an intravenous glucose tolerance test (Supplementary Fig. 1) indicated that glucose-induced insulin secretion was normal after O_3 exposure. Taken together, these results demonstrate that O_3-induced glucose intolerance is due to peripheral IR rather than a deficit in insulin secretion.

To gain insights into the molecular determinants of O_3-induced IR, we assessed activation of the insulin signaling

Table 1—Effect of short-term exposure to O_3 (0.8 ppm, for 16 h) on plasma parameters

	Clean air (*n* = 12)	O_3 (*n* = 12)	Change, %	*P* value
Metabolic parameters				
Fasted glucose, mmol/L	4.3 ± 0.3	5.3 ± 0.2	+23	0.006*
Fasted insulin, μU/mL	11.5 ± 3.2	26.1 ± 4.2	+128	0.018*
HOMA-IR	2.6 ± 0.9	6.3 ± 1.2	+149	0.016*
Triacylglycerols, mmol/L	2.1 ± 0.2	2.2 ± 0.4	+3	0.944
Total cholesterol, mmol/L	1.8 ± 0.3	2.1 ± 0.2	+17	0.184
NEFA, mmol/L	0.53 ± 0.06	0.67 ± 0.06	+26	0.116
Oxidative stress biomarkers				
HNE, nmol/L	7.2 ± 3.5	21.6 ± 2.4	+198	0.038*
HHE, nmol/L	11.3 ± 2.8	38.9 ± 2.5	+244	0.021*
MDA, μmol/L	0.85 ± 0.13	2.24 ± 0.32	+163	0.008*
Carbonyls, nmol/mg	2.78 ± 0.13	4.48 ± 0.15	+61	<0.001*
GSH, mmol/L	1.66 ± 0.26	1.15 ± 0.15	−30	0.124
GSSG, mmol/L	0.13 ± 0.08	0.48 ± 0.15	+276	0.075
GSH-to-GSSG ratio	33.6 ± 9.2	8.0 ± 5.9	−66	0.047*

Data are reported as the mean ± SEM, unless otherwise indicated. Differences between rats exposed to clean air and O_3 were compared using Student *t* test. *Differences were considered significant at the $P < 0.05$ level.

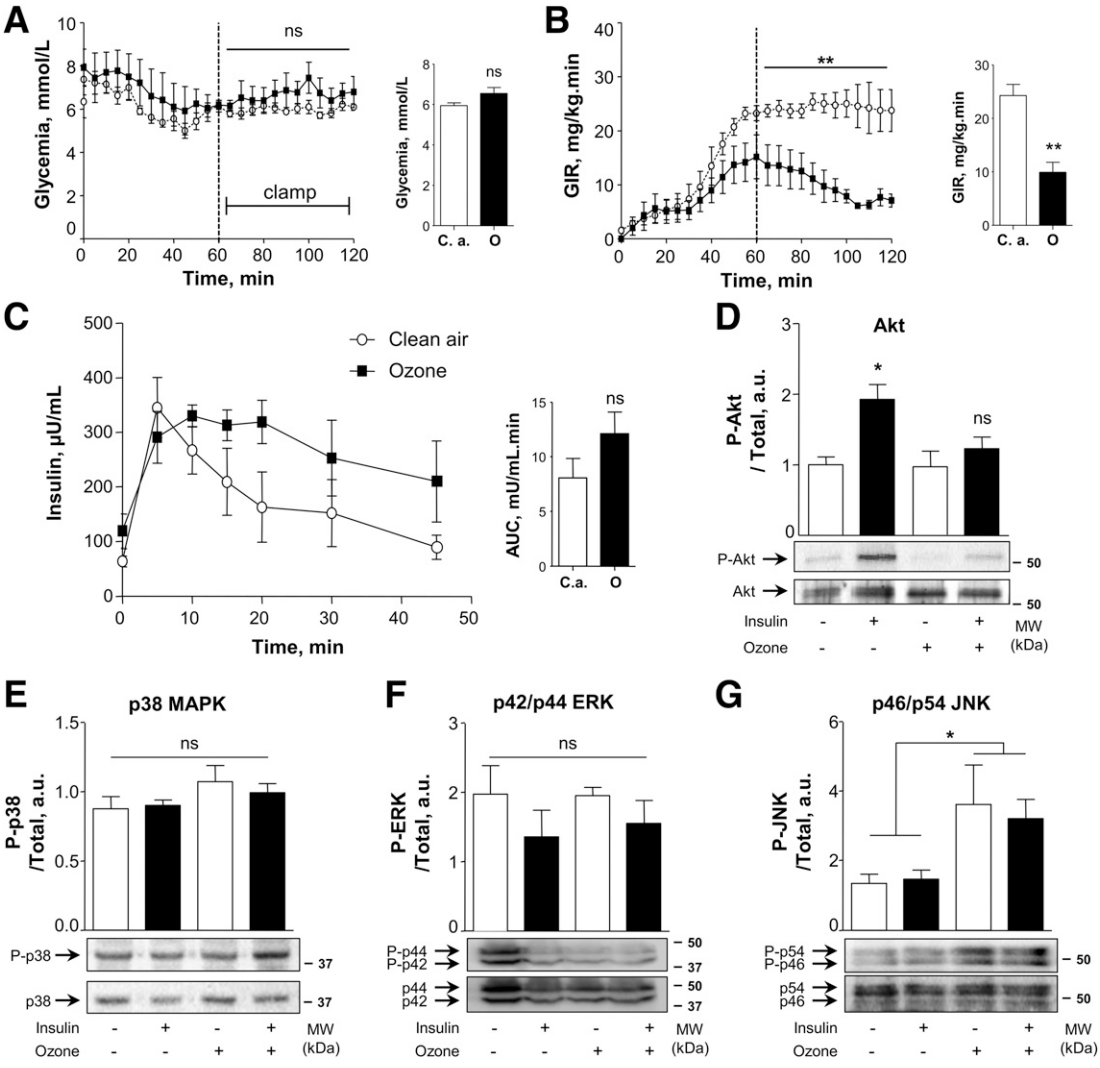

Figure 1—Exposure to O_3 induces IR and the disruption of insulin signaling pathways in skeletal muscle. Rats were exposed to clean air or O_3 (0.8 ppm, for 16 h), as described in RESEARCH DESIGN AND METHODS. Insulin sensitivity was measured using EH clamps in fasting rats. Blood glucose was clamped at 6 mmol/L. Mean glycemia was measured (*A*) and mean GIR was calculated (*B*) as the glucose perfused during the second hour of the clamp that was required to maintain euglycemia (in milligrams per kilogram per minute). All results are reported as the mean ± SEM ($n = 5$). *C*: Plasma insulin concentration was measured after intravenous administration of a nonglucose insulin secretagogue (arginine, 1 g · kg^{-1}, $n = 5$). Note that no difference was found between the two groups at the $P < 0.05$ level. *D*: Rats were stimulated with insulin (0.75 IU/kg i.p.) prior to being killed, and insulin-induced phosphorylation of PKB/Akt was measured in gastrocnemius muscle. Activation of MAPKs p38 protein (*E*), ERK1/2 (*F*), and JNK (*G*) was measured in gastrocnemius muscle. Data are the mean ± SEM for $n = 4$–6. $^*P < 0.05$, $^{**}P < 0.01$, significant difference between control and O_3-exposed rats. C.a., clean air; ns, nonsignificant; O, O_3; P, phorphorylated.

pathway in skeletal muscle. Insulin-induced protein kinase B (PKB)/Akt phosphorylation was significantly impaired in gastrocnemius ($P < 0.01$ vs. control) (Fig. 1*D*) and extensor digitorum longus (data not shown) muscles of O_3 rats, confirming that O_3-induced glucose intolerance is due to skeletal muscle IR. In contrast, insulin signaling was not impaired in liver and white adipose tissue (Supplementary Fig. 2*A* and *B*), suggesting that IR was restricted to skeletal muscle.

Since activation of stress protein kinases can interfere with insulin signaling pathways, we studied the activation of JNK, extracellular signal–related kinase (ERK) 1/2, and p38 mitogen-activated protein kinase (MAPK) in gastrocnemius muscle. O_3 exposure specifically increased the phosphorylation of JNK (5.6-fold, $P < 0.01$), while p38 and ERK remained unaffected, suggesting a particular role of p46/p54 JNK in O_3-induced IR (Fig. 1*E*–*G*). A dose-response experiment (with O_3 concentrations ranging from 0.1 to 0.8 ppm) gave evidence that a significant effect on insulin sensitivity was noticeable from a concentration of 0.3 ppm O_3 (Supplementary Fig. 3).

O_3 Exposure Induces Production of Toxic Mediators in the Lung

As O_3 is too reactive to penetrate deeply into the tissues and reach the bloodstream, we hypothesized that an

oxidative and/or inflammatory insult in the lung might be responsible for the peripheral IR. Animals exposed to O_3 had increased infiltration of cells in the lung (15-fold, $P < 0.001$) (Fig. 2*A*) due to an increase in neutrophils, lymphocytes, and monocytes (Fig. 2*B*). Accordingly, alveolar capillary membrane permeability was increased, as revealed by a markedly increased protein concentration in the BALF of O_3-exposed rats (12-fold, $P < 0.01$) (Fig. 2*C*). Infiltration of immune cells and increased alveolar permeability confirmed that O_3 induced an important inflammatory response in the lung; however, no difference in the number of inflammatory cytokines was found in either BALF or plasma (Supplementary Table 2), suggesting that there was little contribution of inflammation to the remote metabolic effects of O_3 exposure.

O_3 is a strong oxidant, and most of its toxic effects are mediated through free radical reactions. Indeed, lipid peroxidation, measured through thiobarbituric acid–reactive substances (TBARS) concentration, was markedly increased in BALF from O_3-treated animals (threefold, $P < 0.001$) (Fig. 2*D*). HNE and HHE, two reactive lipid aldehydes (among the most cytotoxic products of lipid peroxidation) were increased in BALF from O_3-exposed rats (Fig. 2*E*). Protein carbonyls, end products of oxidative stress, were also significantly increased in the lung (ninefold, $P < 0.001$) (Fig. 2*F*), confirming the oxidative stress in lungs after O_3 exposure. Surprisingly, and unlike inflammation, oxidative stress was not limited to the lung. O_3 exposure induced an increase in many oxidative stress biomarkers in blood (Table 1), such as lipid peroxidation by-products (2.5-, 2.0-, and 1.6-fold increases in HHE, HNE, and MDA concentrations, respectively, $P < 0.05$), and protein carbonyls (by 63%, $P < 0.001$). In good agreement, the GSH-to-GSSG ratio in erythrocytes was decreased in O_3 exposed rats (by 66%, $P < 0.05$). Even more striking was the increase in protein carbonyls in gastrocnemius muscle (3.3-fold, $P < 0.001$) after O_3 exposure (Fig. 2*F*), suggesting that oxidative stress can spread into peripheral tissues and be responsible for the remote effects of O_3.

BALF From O_3 Rats Impairs Insulin-Induced Glucose Uptake and Signaling in C2C12 Myotubes Through Activation of JNK

In order to confirm that toxic mediators produced in the lung could affect peripheral tissues, plasma and BALF samples collected from control and O_3-treated rats were used to treat C2C12 myotubes in vitro. No significant difference in cell viability was observed between control and BALF-treated cells (Supplementary Fig. 4), but a 30-min pretreatment with BALF (10% v/v) from O_3 rats completely abolished the insulin-stimulated [^{3}H]-2-deoxy-D-glucose transport in myotubes (Fig. 3*A*). Accordingly, insulin-induced serine phosphorylation of PKB/Akt (Fig. 3*B*) and tyrosine phosphorylation of insulin receptor substrate-1 (IRS-1) (Fig. 3*C*) were totally inhibited after O_3 BALF exposure compared with clean-air BALF. Taken together, these results demonstrate that BALF from O_3-exposed rats impaired insulin signaling in muscle cells. In good agreement with in vivo experiments, C2C12 myotubes preincubated with BALF from O_3-exposed rats

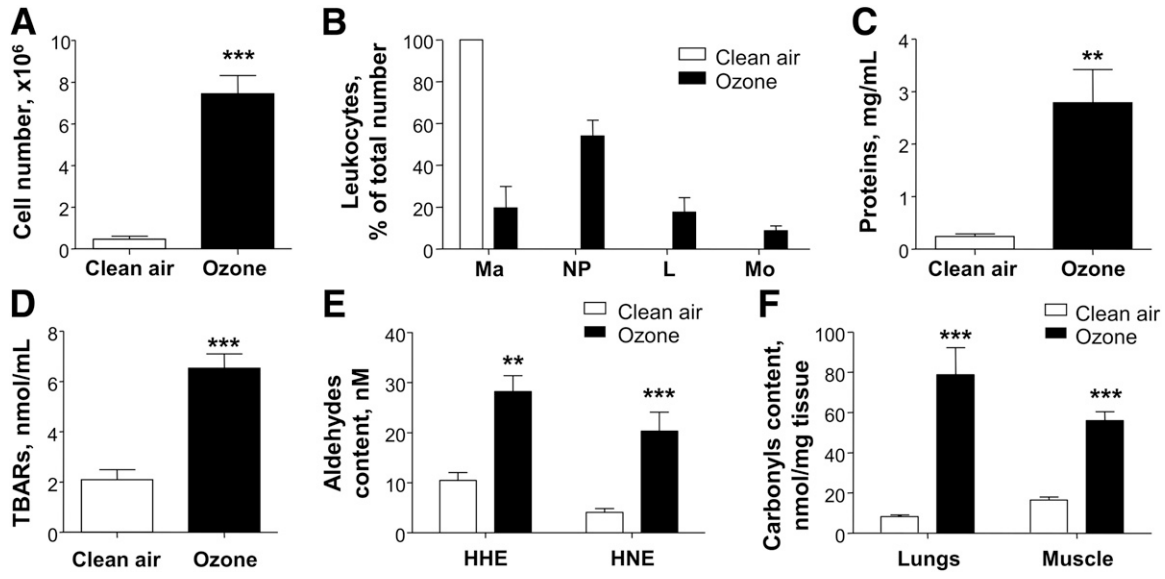

Figure 2—O_3-induced alterations in BALF cell counts and oxidative stress biomarkers. Rats were anesthetized after clean air or O_3 (ozone) exposure, and catheters were placed in the trachea to collect BALF. Total cell count (*A*) and differential cell count (*B*) using May-Grünwald Giemsa staining. Total protein concentration (*C*) and TBARS concentration (*D*) quantified on supernatants. *E*: The lipid aldehydes HNE and HHE were assayed by gas chromatography coupled to mass spectrometry. *F*: Protein carbonyl contents measured in lungs and gastrocnemius muscle. Results are reported as the mean ± SEM for $n = 6$–10. $^{**}P < 0.01$, $^{***}P < 0.005$, significant differences between clean air (open bar) and O_3 (solid bar) animals. L, lymphocytes; Ma, macrophages; Mo, monocytes; NP, neutrophil polynuclears.

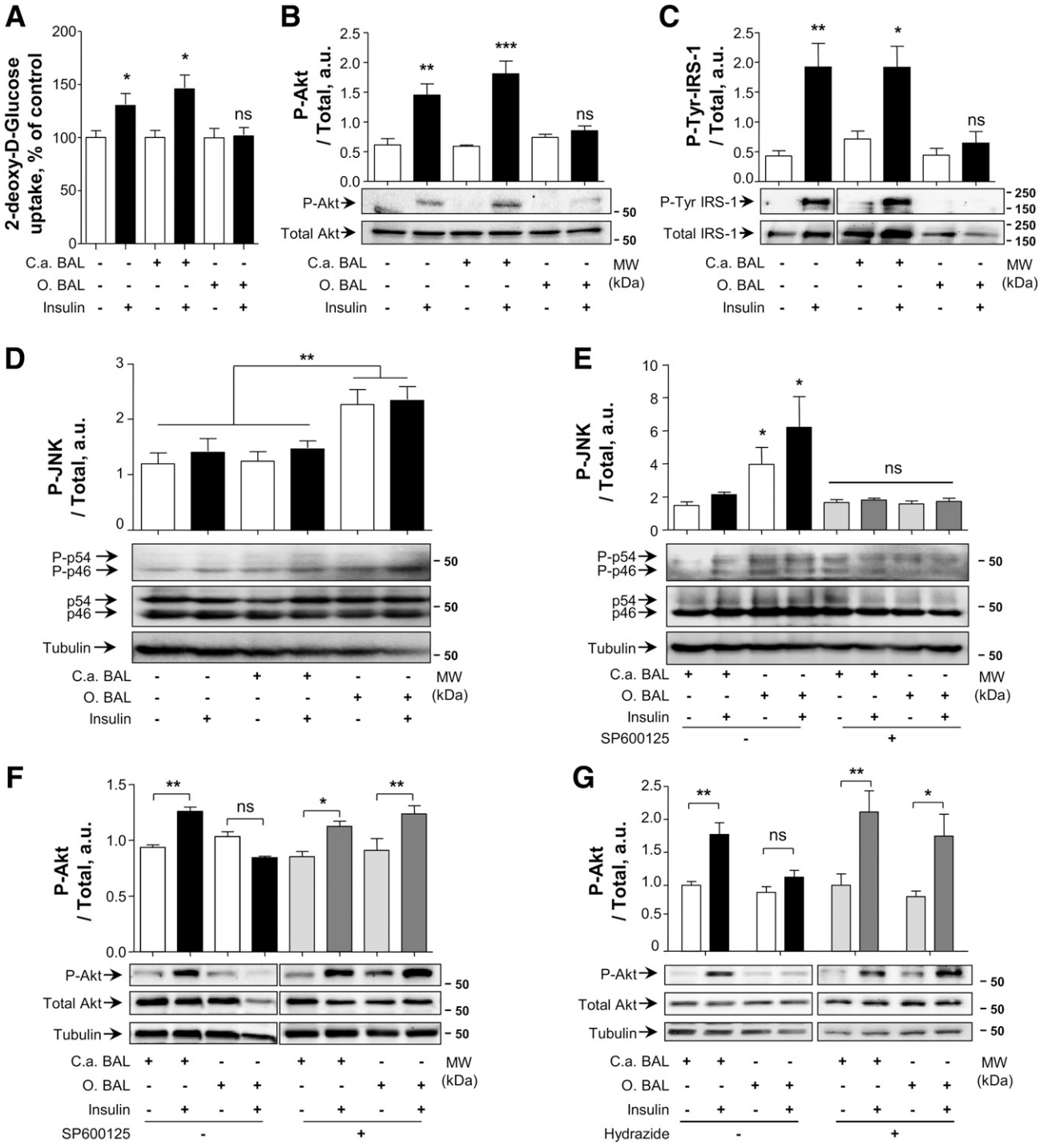

Figure 3—BALF from O_3 rats inhibits insulin-stimulated glucose uptake and disrupts insulin signaling pathways in C2C12 myotubes: role of JNK in O_3-induced IR. C2C12 myotubes were incubated for 30 min with BALF (10%, v/v) from control or O_3-exposed rats and were stimulated by 100 nmol/L insulin for 20 min. *A*: Glucose uptake was measured as the incorporation of [^{3}H]-2-deoxy-glucose into cells. The insulin signaling pathway was explored by Western blotting. O_3 BALF inhibits serine phosphorylation of PKB/Akt (*B*) and tyrosine phosphorylation of IRS-1 (*C*). *D*: Treatment with O_3 BALF induces phosphorylation of JNK. *E* and *F*: JNK inhibitor SP600125 (20 μmol/L, for 1 h) inhibits O_3-BALF prevented JNK activation and restored insulin-stimulated PKB/Akt phosphorylation. *G*: Depletion of lipid aldehydes prevented BALF-induced IR. A hydrazide resin was used as an affinity support for immobilizing lipid aldehydes present in BALF. Note that after treatment with hydrazid resin, the lipid aldehydes (HHE and HNE) in BALF remained undetectable. Data are reported as the mean ± SEM for n = 4–5. $^*P < 0.05$; $^{**}P < 0.01$; $^{***}P < 0.005$. C.a., clean air; MW, molecular weight; ns, nonsignificant; O., O_3; P, phosphorylated.

exhibited a 1.5-fold increase in JNK phosphorylation with or without insulin ($P < 0.05$) (Fig. 3*D*), while no change was observed for ERK1/2 (data not shown). Pretreatment of cells with the JNK inhibitor SP600125 (10 μmol/L, for 1 h) prior to BALF incubation totally inhibited JNK activation (Fig. 3*E*) and restored insulin-induced PKB/Akt phosphorylation (Fig. 3*F*), pointing out the specific role of JNK in mediating the effects of BALF in C2C12 myotubes. In contrast with BALF, rat plasma decreased C2C12 cell viability (Supplementary Table 3). Insulin-induced serine phosphorylation of PKB/Akt (Supplementary Fig. 5*A*) was, however, totally inhibited after incubation with plasma from O_3-exposed rats, while JNK phosphorylation was increased (Supplementary Fig. 5*B*). These data fully confirm the results observed in experiments with BALF. Lipid aldehyde levels, which were increased in both BALF and plasma from O_3-exposed rats, are potent electrophiles that could mediate the effects of O_3 beyond the air/tissue interface. To support this view, we used a hydrazide resin as an affinity support for immobilizing lipid aldehydes present in BALF and incubated C2C12 cells with "aldehyde-depleted BALF." After treatment with hydrazide resin, the concentrations of HHE and HNE in BALF remained lower than the limit of detection. C2C12 muscle incubated with aldehyde-depleted BALF did not display any disruption of the insulin pathway, as evidenced by insulin-induced serine 473 phosphorylation of PKB/Akt (Fig. 3*G*), suggesting that lipid aldehydes, produced in the lung under the action of O_3, could contribute to IR.

Oxidative Stress Is a Major Contributor to O_3-Induced IR

As oxidative stress seemed to be a major determinant of the noxious effects of O_3, we studied the ability of the antioxidant NAC (225 mg · kg $^{-1}$ · day^{-1}, for 10 days) to prevent O_3-induced IR in rat. NAC pretreatment significantly increased the GSH-to-GSSG ratio (1.5-fold, $P = 0.03$) in muscle (Supplementary Fig. 6) and prevented its decrease after O_3 exposure. NAC treatment prevented the decrease in insulin sensitivity (Fig. 4*A*) observed after overnight O_3 exposure, as well as the increase in protein carbonyl content in lung and muscle (Fig. 4*B*) and the TBARS increase in BALF (Fig. 4*C*). Interestingly, NAC pretreatment failed to prevent lung inflammation, as evidenced by increased protein concentrations (ninefold, $P < 0.01$) and cell counts (eightfold, $P < 0.001$) in BALF (Fig. 4*D* and *E*), suggesting that the inflammatory components of the noxious effects of O_3 were upstream of oxidative stress. Finally, treatment of C2C12 myotubes with BALF from rats pretreated with NAC prior to O_3 exposure neither impaired insulin-induced Akt phosphorylation (3.6-fold, $P < 0.001$) (Fig. 4*F*) nor increased JNK phosphorylation (Fig. 4*G*), demonstrating that oxidative stress is a major mediator of the peripheral effects of O_3 on muscle insulin sensitivity.

O_3 Triggers Activation of Discrete/Selective ER Stress Pathways

Under conditions of oxidative stress, the accumulation of oxidized lipids or advanced oxidation protein by-products can induce ER stress and JNK activation. O_3 exposure, however, triggered a limited effect on ER stress protein gene expression in rat gastrocnemius muscles (Fig. 5*A*) since changes were restricted to the overexpression of Atf6 (increase of 106%, $P < 0.01$) and Ire1a (increase of 36%, $P = 0.06$) genes, while the expression of other ER stress protein genes such as Bip (Gpr78), Perk, Eif2s1, or Atf4 remained unaltered. O_3-exposed rats exhibited a modest post-translational activation of inositol-requiring protein-1α (IRE-1α) (1.6-fold, $P = 0.1$) (Fig. 5*B*), but not PERK (data not shown), in their gastrocnemius muscles. Incubation of C2C12 myotubes with BALF from O_3 rats recapitulated the activation of IRE-1α (Fig. 5*C*) (1.6-fold, $P < 0.05$). To confirm the activation of JNK downstream of ER stress, we pretreated C2C12 myotubes with a chemical chaperone, 4-PBA (10 mmol/L, for 1 h), to prevent ER stress. Pretreatment with PBA prevented the O_3-induced activation of JNK (Fig. 5*D*) and restored the activation of PKB/Akt in response to insulin (Fig. 5*E*). These results were confirmed in vivo, as PBA pretreatment (150 mg · kg^{-1} · day^{-1}, for 4 days) significantly prevented O_3-induced IR, as measured with an ITT (Fig. 5*F*). Taken together, these data demonstrate that the induction of selective ER stress pathways in skeletal muscle could contribute to O_3-induced IR.

Recovery From O_3-Induced IR

O_3 pollution peaks are transient and rarely last for more than a few days. To decipher how long O_3-induced IR could persist after the end of the exposure, intraperitoneal ITTs were performed immediately after O_3 exposure, and 24, 72, and 96 h later. Strikingly, even 96 h after O_3 exposure, animals exhibited a significant impairment in insulin sensitivity (Fig. 6*A*). The K_{ITT} was lower in all O_3-exposed groups compared with control rats ($n = 5$, $P < 0.05$). In skeletal muscle, JNK phosphorylation also lasted for up to 96 h (Fig. 6*B*) after O_3 exposure, while ER stress (IRE-1) nearly returned to baseline after 24 h (Fig. 6*C*). In contrast, oxidative stress and inflammatory markers in BALF returned to baseline in 24–48 h (Fig. 6*D*–*G*). These results show that an overnight acute exposure to O_3 can induce defects in skeletal muscle and impair insulin sensitivity for up to 3 days.

Subchronic Exposure to O_3 Induces IR

Rats underwent a subchronic exposure to a lower dose of O_3 (0.25 ppm, 12 h/day) for 4 days. We deliberately chose an intermittent O_3 exposure to take into account the day-to-night variations that generally characterize O_3 pollution in urban areas. Of note, long-term exposure to O_3 (0.25 ppm), as observed with the acute exposure study, yielded pulmonary inflammation, oxidative stress, and IR (Fig. 7).

DISCUSSION

Diet and sedentary lifestyle are the most common risk factors for cardiometabolic disorders; however, recent observations have also shown a strong association between other

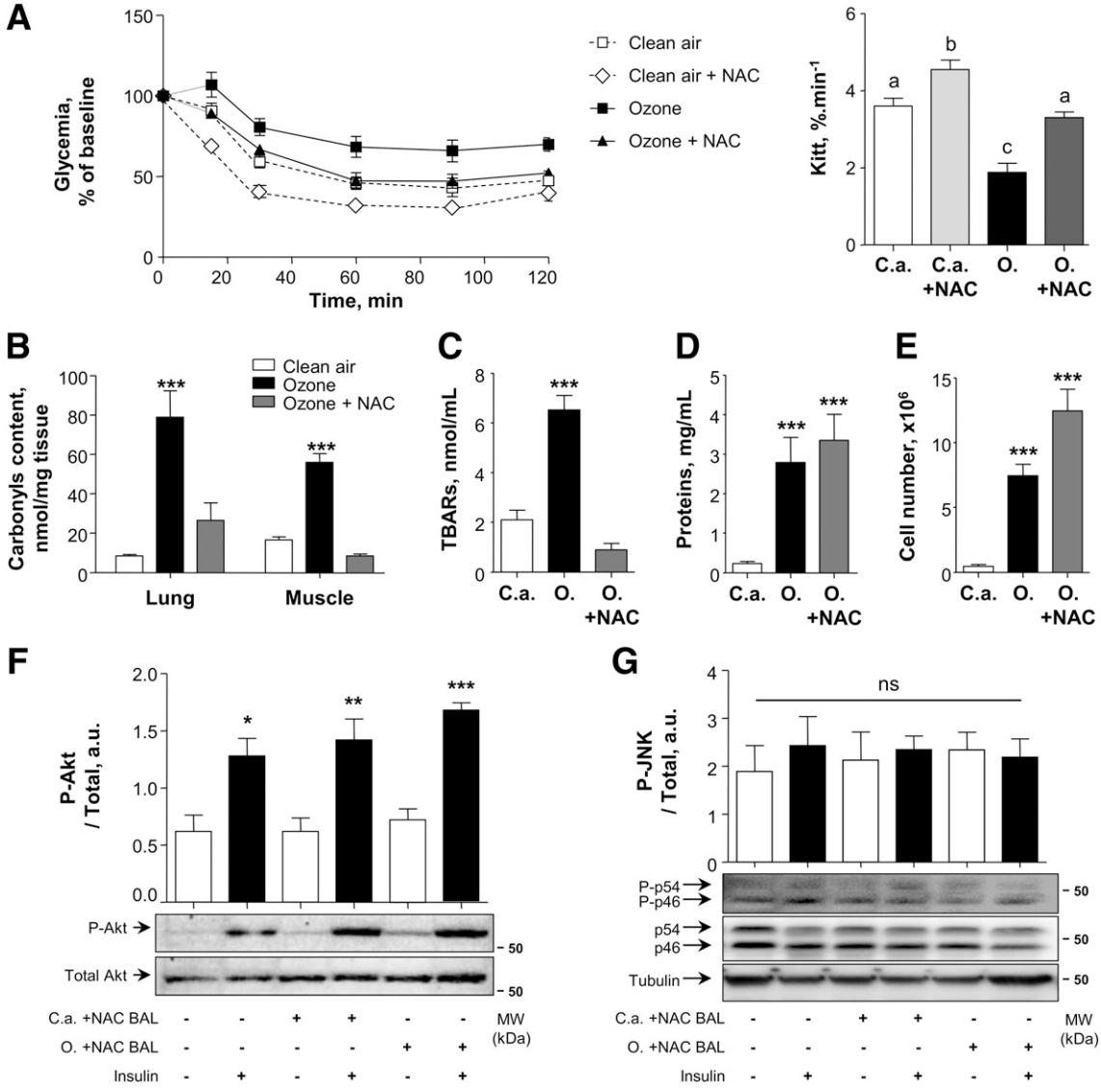

Figure 4—The antioxidant NAC prevented O_3-induced disruption of insulin signaling pathways. Rats were given NAC (225 mg · kg^{-1}) for 10 days prior to O_3 exposure. Insulin sensitivity was explored using ITT. *A*: Blood glucose concentration was measured after intraperitoneal injection of insulin (0.5 IU/kg) in fasting rats, and plasma K_{ITT} was calculated. Results are expressed as the mean ± SEM for $n = 5$ rats. $^{**}P < 0.01$, $^{***}P < 0.005$. Different letters (a, b, and c) indicate a significant difference at $P < 0.05$. Carbonyl content in muscle and lung (*B*), TBARS concentration (*C*), total protein concentration (*D*), and total cell count (*E*) in BALF ($n = 5$). $^{**}P < 0.01$, $^{***}P < 0.005$. C2C12 myotubes were incubated for 30 min with BALF (10%, v/v) from rats pretreated with NAC and exposed to O_3, and stimulated by 100 nmol/L insulin for 20 min. Insulin-induced phosphorylation of PKB/Akt (*F*) and JNK (*G*) was measured by Western blotting. Results are reported as the mean ± SEM for $n = 4$. $^{*}P < 0.05$; $^{**}P < 0.01$; $^{***}P < 0.005$. C.a., clean air; MW, molecular weight; ns, nonsignificant; O., O_3; P, phosphorylated.

environmental factors such as air pollution (especially from traffic-related sources) and T2D (5). More and more recent cohort studies indeed associate traffic-related air pollution with the incidence of T2D. For instance, exposure to NO_2 is associated with diabetes prevalence among women (33) and with the development of diabetes in healthy individuals (4). PM pollution, consisting of airborne particles in solid or liquid form of <10 μm (PM_{10}), is also associated with incident T2D among elderly women (3). Although most aspects of the association of metabolic diseases with air pollution remain to be elucidated, these observations are of importance, given the high levels of airborne pollutants in urbanized environments, which could represent an underappreciated but critical link between industrialization and the increased incidence of metabolic diseases (34). Since it is produced from other pollutants, O_3 is the reflection of advanced polluted air environments and only recently has attracted the attention of scientists. O_3 is a major photochemical pollutant in urban areas, produced from the action of UV rays on volatile organic compounds or NO_x (NO, NO_2) emitted during the combustion of fossil fuels by automobile exhausts and industrial activities (6). As with PM and NO_2, O_3 is also associated with increased fasting glucose

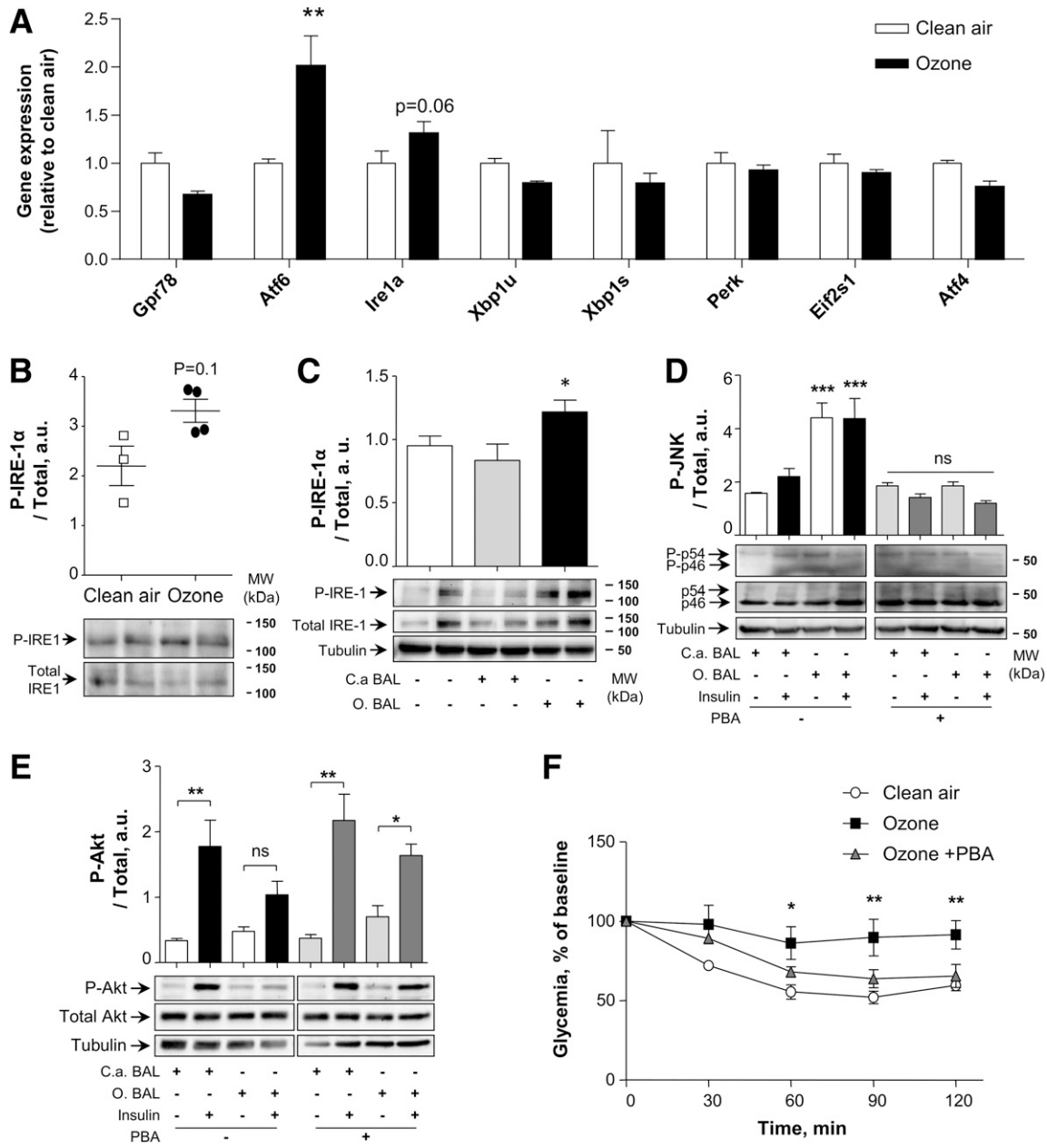

Figure 5—O_3-induced ER stress mediates JNK activation and IR. *A*: Gene expression of major ER stress markers (Gpr78, Atf6, Ire1α, spliced Xbp1, Perk, Eif2s1, and Atf4) was measured by real-time RT-PCR. *B*: Activation of ER stress protein IRE-1α was explored in gastrocnemius muscle by Western blotting. Results are reported as the mean ± SEM (n = 4). $^*P < 0.05$,$^{**}P < 0.01$. C2C12 myotubes were incubated for 30 min with BALF (10%, v/v) from control or O_3-exposed rats and were stimulated by 100 nmol/L insulin for 20 min. *C*: Activation of ER stress protein IRE-1α was explored by Western blotting. Results are reported as the mean ± SEM (n = 8 in each group). $^*P < 0.05$. C2C12 myotubes were pretreated with the chemical chaperone 4-PBA (10 mmol/L, for 1 h) prior to incubation with BALF (10%, v/v). Pretreatment with PBA prevented BALF-induced JNK activation (*D*) and reversed the inhibition of insulin-stimulated PKB/Akt phosphorylation (*E*). Data are reported as the mean ± SEM for n = 4–5. $^*P < 0.05$, $^{**}P < 0.01$, $^{***}P < 0.005$. Rats were given 4-PBA (150 mg · kg^{-1} · day^{-1}) for 4 days prior to O_3 exposure. Insulin sensitivity was explored using ITT. *F*: Blood glucose concentration was measured after intraperitoneal injection of insulin (0.5 IU/kg) in fasting rats. Results are expressed as the mean ± SEM for n = 5 rats. C.a., clean air; ns, nonsignificant; O., O_3; P, phosphorylated.

and insulin levels, and HOMA indices in elderly (35). The association of O_3 with these parameters is stronger among participants with a history of diabetes or increased susceptibility to oxidative stress, suggesting that O_3 could boost the development of diabetes.

The major finding of the current study is that a realistic acute O_3 exposure induces peripheral IR in vivo. This result was confirmed using the following three different methods: HOMA-IR, insulin and glucose tolerance tests, and the gold standard EH clamp technique. Skeletal

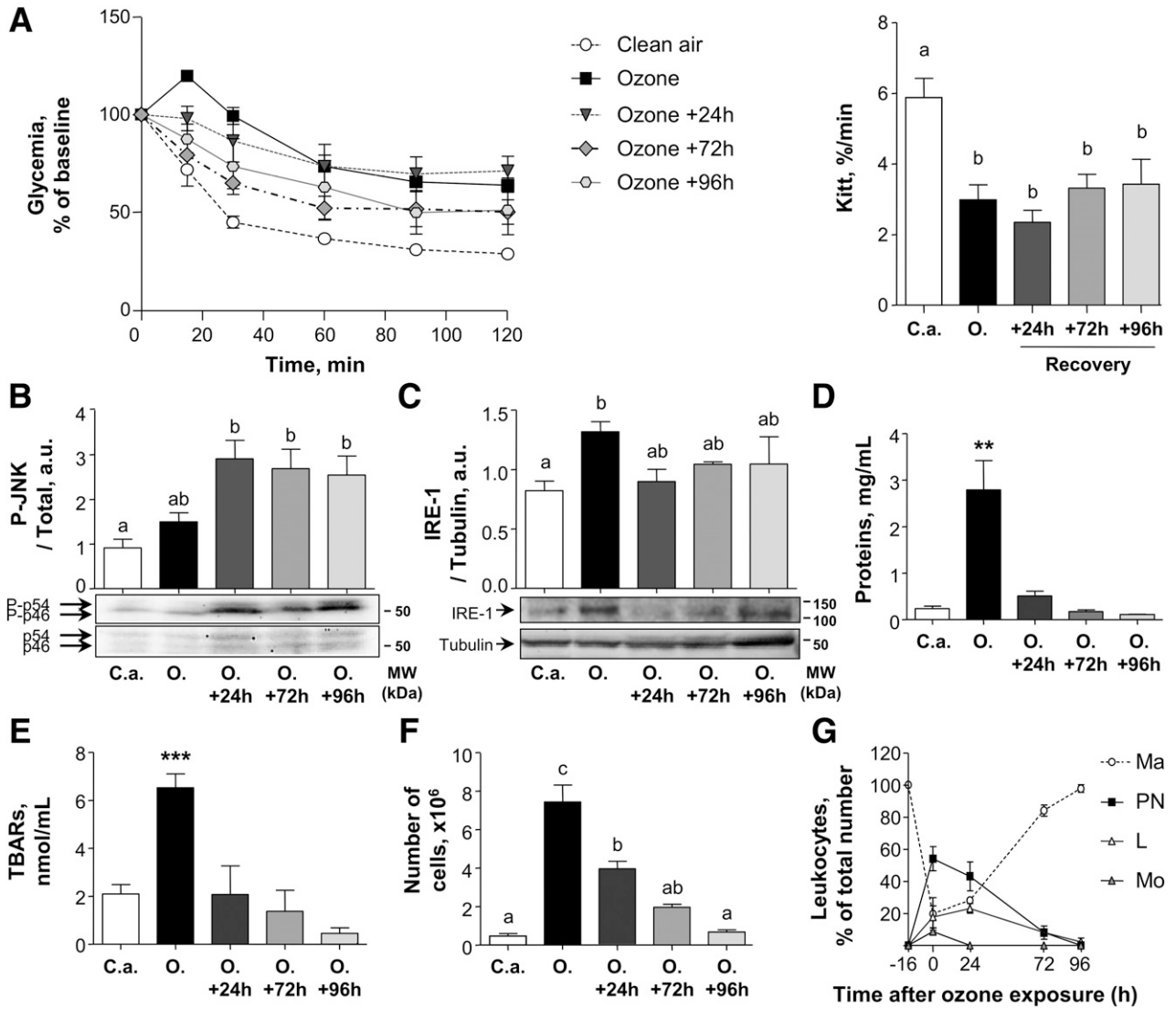

Figure 6—Reversibility of O_3-induced IR. Rats were exposed to clean air or to ozone as described previously and insulin sensitivity was studied with intraperitoneal ITT, immediately, and 24, 72, and 96 h after exposure. *A*: Blood glucose level was measured after intraperitoneal injection of insulin (0.5 IU/kg) to fasting rat and plasmatic K_{ITT} during the ITT was calculated. Results are reported as the mean ± SEM (n = 5 in each group); different letters (a and b) indicate a significant difference at $P < 0.05$. Gastrocnemius muscles were dissected out immediately after; and 24, 72, and 96 h after O_3 exposure; and JNK phosphorylation (*B*) and ER stress protein IRE-1α (*C*) levels were analyzed by Western blotting. BALF was sampled just before the killing of the rats; immediately after; and 24, 72, and 96 h after exposure; and total protein concentration (*D*), TBARS concentration (*E*), total cell count (*F*), and differential cell count (*G*) were analyzed. Results are reported as the mean ± SEM for n = 4–10. $^{**}P < 0.01$; $^{***}P < 0.005$. C.a., clean air; L, lymphocytes; Ma, macrophages; Mo, monocytes; MW, molecular weight; NP, neutrophil polynuclears; ns, nonsignificant; O., O_3; P, phosphorylated.

muscle is the major tissue responsible for insulin-stimulated glucose disposal in lean individuals and, as such, has been identified to be pivotal for the development of IR (36,37). The measurement of insulin-induced PKB/Akt phosphorylation in skeletal muscles (gastrocnemius and extensor digitorum longus) further confirmed that O_3 induced a selective defect in muscle insulin sensitivity compared with liver and adipose tissue (Fig. 1).

The O_3 Exposure Rat Model

Ground-level O_3 air pollution can often reach 0.18 ppm (i.e., 360 μg/m^3), corresponding to level 3 of the alert threshold established by European Directive 2008/50/CE. This concentration of O_3 can cause a number of respiratory health problems, and can worsen asthma, allergies, and chronic obstructive pulmonary diseases (38). O_3 was primarily studied in this context, and a rat model that mimics O_3 exposure was developed and extensively characterized. In particular, it was demonstrated that rats remove a smaller fraction of their inhaled amount of O_3 (40–47%) than humans (75% with large interindividual variations) (39,40). As a consequence, the toxicity of O_3 observed for a given concentration in rats strongly underestimates the effect observed for the

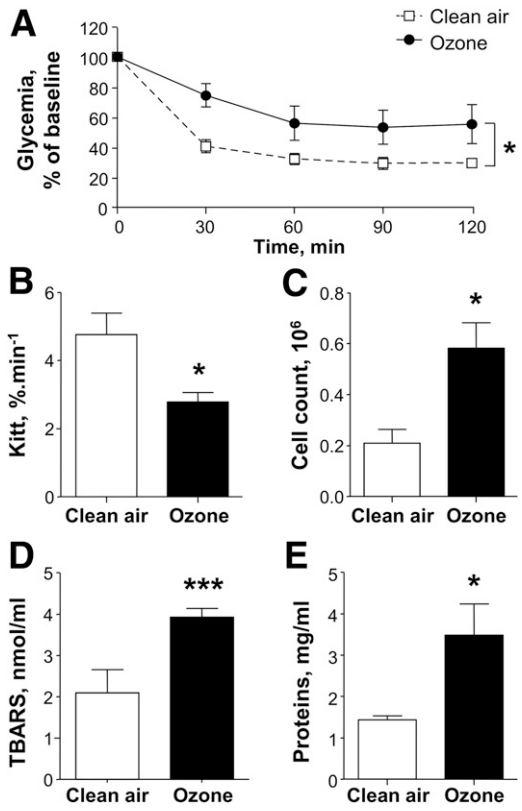

Figure 7—Subchronic exposure to O_3 (0.25 ppm, 12 h/day, for 4 days) induces IR. Rats were exposed 12 h/day for 4 days to clean air or O_3 (0.25 ppm). Insulin sensitivity was estimated using ITT. Blood glucose levels (*A*) were measured after intraperitoneal injection of insulin (0.5 IU/kg) in fasting rats, and the plasma K_{ITT} (*B*) measured during the ITT was calculated. Results are reported as the mean ± SEM for $n = 7$ animals. Rats were anesthetized after clean air or O_3 exposure, and catheters were placed in the trachea to collect BALF. Total cell count (*C*), TBARS concentration (*D*), and total protein concentration (*E*) were quantified on supernatants. Results are reported as the mean ± SEM for $n = 5$. $^*P < 0.05$, $^{***}P < 0.005$, significant differences between animals exposed to clean air (open bar) and O_3 (solid bar).

same concentration in humans, and thus, the effects observed in humans are comparable to those produced in rats exposed to a fivefold higher O_3 concentration (41). The concentrations chosen in the current study (0.25–0.8 ppm) are therefore realistic to mimic the actual levels of O_3 commonly encountered in urban areas during pollution peaks. Of note, IR was noticeable from concentrations of 0.25–0.3 ppm O_3 (Supplementary Fig. 3).

O_3 Induces Production of Toxic Lung Mediators

O_3 is too reactive to penetrate deeply into the tissues and reach the bloodstream (42). Instead, it promptly reacts with molecules of lung-lining fluid and/or with plasma membranes of airway epithelial cells to produce lipid aldehydes and lipid ozonation products, which are highly susceptible to initiating pathophysiological cascades (42). Aldehydes and/or lipid ozonation products have a lower reactivity and longer $t_{1/2}$ than O_3 itself and could mediate the effects of O_3 beyond the air/tissue interface. To support the idea of O_3-induced lung mediators that trigger IR, we recapitulated the effects of O_3 in vitro by treating C2C12 myotubes with BALF. Muscle cells treated with BALF from O_3-exposed rats exhibited an inhibition of insulin-stimulated glucose uptake and Akt phosphorylation, similar to in vivo O_3 exposure (Fig. 3). Moreover, partial inhibition of insulin-induced PKB/Akt phosphorylation could also be achieved with BALF from control animals submitted to in vitro ozonation (Supplementary Fig. 7). As most of these factors are likely oxidation products, this is consistent with previous reports (43,44) showing that lipid ozonation products such as cholesterol secoaldehydes have deleterious effects, inducing apoptosis in cardiomyocytes and neurons. In addition, publications by us and others (32,45,46) showed that lipid aldehydes and carbonyl stress trigger IR in muscle cells and adipocytes. Our results support that it is the reaction of O_3 with components of lung-lining fluid and/or surfactant that produces toxic by-products/factors that are able to induce IR. We further demonstrated that lipid aldehydes (e.g., HNE and HHE) produced under O_3 exposure could participate in these extrapulmonary effects of O_3 (Fig. 3*G*).

O_3-Induced Lung Inflammation and Systemic Oxidative Stress

The lung is obviously the first tissue affected by O_3, and we indeed observed a large increase in protein concentration and immune cell infiltration, which are hallmarks of lung inflammation (Fig. 2). Although inflammation seems to be an important component of the O_3 response, it is limited to the lung, as overnight exposure to O_3 yielded only minor changes in systemic inflammatory cytokine and prostaglandin levels. In addition, the treatment of rats with the antioxidant NAC does not prevent lung inflammation (Fig. 4) but does restore insulin sensitivity in the muscle. Furthermore, recovery experiments showed that infiltration of the lung by immune cells resolves after 24 h, whereas muscle IR lasts for up to 3 days (Fig. 6). Taken together, these results strongly suggest that inflammation is not directly responsible for the defects observed in muscle. This is consistent with a recent study (14) showing that lung inflammation was not a requirement for the production of circulating vasoactive factors after O_3 exposure. Lung inflammation is, however, an important source of radical species (47) and may contribute to the oxidative chain reactions induced by O_3. We indeed observed that rats exposed to O_3 exhibit a systemic increase in blood reactive aldehyde levels (Table 1), as well as an increase in muscle carbonyl levels. In addition, pretreatment of rats with the antioxidant NAC prevented oxidative stress, carbonylation of muscle proteins, and IR, strongly suggesting that the systemic effects of O_3 are due to oxidative stress (Fig. 4).

Characterization of the Effect of O_3 in Muscle Cells: ER Stress and JNK

In response to several types of stress, the aggregation of misfolded or abnormal proteins leads to ER stress, consequently triggering the unfolded protein response (UPR) pathways in order to restore ER homeostasis. This response can be induced by pollutants and is involved in PM toxicity. In vitro studies (48) have demonstrated that $PM_{2.5}$ (PM <2.5 μm) induces ER stress and significantly increases the UPR-associated proteins activating transcription factor-4, HSP70 and HSP90, and BiP. ER stress has been proposed to play a central role in the development of IR in liver and adipose tissue (49), and, indeed, the UPR intersects with a variety of inflammatory and stress-signaling systems, including the nuclear factor-κB and JNK pathways, as well as oxidative stress responses, all of which may influence lipid and glucose metabolism (49). Our study demonstrates that exposure to O_3 in vivo or to BALF from O_3-exposed rats in vitro triggers a modest activation of ER stress pathways in muscle, mostly restricted to the IRE1-α pathway. Using the chemical chaperone 4-PBA, which prevents ER stress and ER stress–mediated activation of JNK (50), we demonstrated in vivo and in vitro that *1*) activation of selective ER stress pathways could contribute to the O_3-induced IR in muscle cells and *2*) JNK activation is downstream of the ER stress activation in this context (Fig. 5).

Whole-body IR can be a consequence of defects in the canonical insulin signaling pathway IRS-1–phosphatidylinositol 3-kinase–PKB/Akt. Increased serine phosphorylation of IRS-1 is indeed triggered by many diabetogenic factors, especially through the stress signaling pathways that have been shown to contribute to the development of IR (51). $PM_{2.5}$ exposure activates JNK and downregulates the IRS1-mediated signaling in the liver, leading to glucose intolerance and IR (52). In addition, specific overexpression of a constitutively active JNK in skeletal muscle has been shown to be sufficient to induce whole-body IR through impairment of insulin signaling (53). In our rat model, O_3 is responsible for a specific activation of JNK signaling in muscle, either after in vivo exposure or after treatment with BALF from O_3-exposed rats. The inhibition of JNK can fully restore the impaired insulin-induced PKB/Akt phosphorylation, demonstrating the important role of JNK in O_3-induced IR (Fig. 3).

In summary, we report here that O_3 plays a causative role in the development of IR and that a realistic, short-term exposure to O_3 causes whole-body IR that lasts for up to 3 days. This alarming phenotype is due to the production of lung mediators that induce oxidative stress and the subsequent activation of JNK in skeletal muscle, therefore disrupting insulin-induced signaling and glucose uptake. Air pollutants generally occur in complex mixtures that create the potential for synergistic effects among pollutants and may worsen their pathological properties. Our results suggest that nontraditional factors such as O_3 pollution could synergize with other dominant factors (obesity and sedentary lifestyle) to accelerate the propensity for T2D and that chaperone molecules or antioxidants could protect susceptible people from complications induced by O_3 pollution peaks.

Acknowledgments. The authors thank Dr. Kevin P. Foley (Cell Biology Program, The Hospital for Sick Children, Toronto, ON, Canada) for proofreading and corrections.

Funding. This work was supported by the Institut National de la Santé et de la Recherche Médicale and the Institut National des Sciences Appliquées de Lyon. R.E.V., N.J.P., B.Z., and M.L.C. were supported by grants from the French Ministère de la Recherche et de la Technologie. L.K. held a fellowship from Fondation pour la Recherche Médicale.

Duality of Interest. No potential conflicts of interest relevant to this article were reported.

Author Contributions. R.E.V., N.J.P., and C.O.S. researched the data and wrote the manuscript. B.Z., M.L.C., M.G., and A.G. researched the data, and reviewed and edited the manuscript. L.K., S.P., M.-A.C., and J.R. researched the data. R.E.V., N.J.P., and C.O.S. are the guarantors of this work and, as such, had full access to all the data in the study and take responsibility for the integrity of the data and the accuracy of the data analysis.

References

1. Bhatnagar A. Could dirty air cause diabetes? Circulation 2009;119:492–494
2. Willett WC. Balancing life-style and genomics research for disease prevention. Science 2002;296:695–698
3. Krämer U, Herder C, Sugiri D, et al. Traffic-related air pollution and incident type 2 diabetes: results from the SALIA cohort study. Environ Health Perspect 2010;118:1273–1279
4. Andersen ZJ, Raaschou-Nielsen O, Ketzel M, et al. Diabetes incidence and long-term exposure to air pollution: a cohort study. Diabetes Care 2012;35:92–98
5. Raaschou-Nielsen O, Sørensen M, Ketzel M, et al. Long-term exposure to traffic-related air pollution and diabetes-associated mortality: a cohort study. Diabetologia 2013;56:36–46
6. Finlayson-Pitts BJ, Pitts JN Jr. Tropospheric air pollution: ozone, airborne toxics, polycyclic aromatic hydrocarbons, and particles. Science 1997;276:1045–1052
7. Akimoto H. Global air quality and pollution. Science 2003;302:1716–1719
8. Eckel SP, Louis TA, Chaves PHM, Fried LP, Margolis AHG. Modification of the association between ambient air pollution and lung function by frailty status among older adults in the Cardiovascular Health Study. Am J Epidemiol 2012;176:214–223
9. Altuğ H, Gaga EO, Döğeroğlu T, et al. Effects of air pollution on lung function and symptoms of asthma, rhinitis and eczema in primary school children. Environ Sci Pollut Res Int 2013;20:6455–6467
10. Soulage C, Perrin D, Cottet-Emard J-M, Pequignot J, Dalmaz Y, Pequignot J-M. Central and peripheral changes in catecholamine biosynthesis and turnover in rats after a short period of ozone exposure. Neurochem Int 2004;45:979–986
11. Martínez-Lazcano JC, González-Guevara E, del Carmen Rubio M, et al. The effects of ozone exposure and associated injury mechanisms on the central nervous system. Rev Neurosci 2013;24:337–352
12. Laskin DL, Pendino KJ, Punjabi CJ, Rodriguez del Valle M, Laskin JD. Pulmonary and hepatic effects of inhaled ozone in rats. Environ Health Perspect 1994;102(Suppl. 10):61–64
13. Tankersley CG, Georgakopoulos D, Tang W-Y, Abston E, Bierman A, Sborz N. Effects of ozone and particulate matter on cardiac mechanics: role of the atrial natriuretic peptide gene. Toxicol Sci 2013;131:95–107

14. Robertson S, Colombo ES, Lucas SN, et al. CD36 mediates endothelial dysfunction downstream of circulating factors induced by O3 exposure. Toxicol Sci 2013;134:304–311
15. Dalle-Donne I, Rossi R, Colombo R, Giustarini D, Milzani A. Biomarkers of oxidative damage in human disease. Clin Chem 2006;52:601–623
16. Evans JL, Maddux BA, Goldfine ID. The molecular basis for oxidative stress-induced insulin resistance. Antioxid Redox Signal 2005;7:1040–1052
17. Bashan N, Kovsan J, Kachko I, Ovadia H, Rudich A. Positive and negative regulation of insulin signaling by reactive oxygen and nitrogen species. Physiol Rev 2009;89:27–71
18. Rains JL, Jain SK. Oxidative stress, insulin signaling, and diabetes. Free Radic Biol Med 2011;50:567–575
19. Evans JL, Goldfine ID, Maddux BA, Grodsky GM. Are oxidative stress-activated signaling pathways mediators of insulin resistance and beta-cell dysfunction? Diabetes 2003;52:1–8
20. Ceriello A, Motz E. Is oxidative stress the pathogenic mechanism underlying insulin resistance, diabetes, and cardiovascular disease? The common soil hypothesis revisited. Arterioscler Thromb Vasc Biol 2004;24:816–823
21. Bocci V, Borrelli E, Travagli V, Zanardi I. The ozone paradox: ozone is a strong oxidant as well as a medical drug. Med Res Rev 2009;29:646–682
22. Lodovici M, Bigagli E. Oxidative stress and air pollution exposure. J Toxicol 2011;2011:487074
23. Sunil VR, Vayas KN, Massa CB, Gow AJ, Laskin JD, Laskin DL. Ozone-induced injury and oxidative stress in bronchiolar epithelium are associated with altered pulmonary mechanics. Toxicol Sci 2013;133:309–319
24. Moulton PV, Yang W. Air pollution, oxidative stress, and Alzheimer's disease. J Environ Public Health 2012;2012:472751
25. Perepu RSP, Dostal DE, Garcia C, Kennedy RH, Sethi R. Cardiac dysfunction subsequent to chronic ozone exposure in rats. Mol Cell Biochem 2012;360:339–345
26. Bass V, Gordon CJ, Jarema KA, et al. Ozone induces glucose intolerance and systemic metabolic effects in young and aged Brown Norway rats. Toxicol Appl Pharmacol 2013;273:551–560
27. Perrin D, Soulage C, Pequignot JM, Géloën A. Resistance to obesity in Lou/C rats prevents ageing-associated metabolic alterations. Diabetologia 2003;46:1489–1496
28. Koppe L, Pillon NJ, Vella RE, et al. p-Cresyl sulfate promotes insulin resistance associated with CKD. J Am Soc Nephrol 2013;24:88–99
29. Ohkawa H, Ohishi N, Yagi K. Reaction of linoleic acid hydroperoxide with thiobarbituric acid. J Lipid Res 1978;19:1053–1057
30. Calzada C, Colas R, Guillot N, et al. Subgram daily supplementation with docosahexaenoic acid protects low-density lipoproteins from oxidation in healthy men. Atherosclerosis 2010;208:467–472
31. Levine RL, Wehr N, Williams JA, Stadtman ER, Shacter E. Determination of carbonyl groups in oxidized proteins. Methods Mol Biol 2000;99:15–24
32. Pillon NJ, Croze ML, Vella RE, Soulère L, Lagarde M, Soulage CO. The lipid peroxidation by-product 4-hydroxy-2-nonenal (4-HNE) induces insulin resistance in skeletal muscle through both carbonyl and oxidative stress. Endocrinology 2012;153:2099–2111
33. Brook RD, Jerrett M, Brook JR, Bard RL, Finkelstein MM. The relationship between diabetes mellitus and traffic-related air pollution. J Occup Environ Med 2008;50:32–38
34. Liu C, Ying Z, Harkema J, Sun Q, Rajagopalan S. Epidemiological and experimental links between air pollution and type 2 diabetes. Toxicol Pathol 2013;41:361–373
35. Kim JH, Hong Y-C. GSTM1, GSTT1, and GSTP1 polymorphisms and associations between air pollutants and markers of insulin resistance in elderly Koreans. Environ Health Perspect 2012;120:1378–1384
36. DeFronzo RA, Gunnarsson R, Björkman O, Olsson M, Wahren J. Effects of insulin on peripheral and splanchnic glucose metabolism in noninsulin-dependent (type II) diabetes mellitus. J Clin Invest 1985;76:149–155
37. Nolan CJ, Damm P, Prentki M. Type 2 diabetes across generations: from pathophysiology to prevention and management. Lancet 2011;378:169–181
38. Medina-Ramón M, Zanobetti A, Schwartz J. The effect of ozone and PM10 on hospital admissions for pneumonia and chronic obstructive pulmonary disease: a national multicity study. Am J Epidemiol 2006;163:579–588
39. Wiester MJ, Williams TB, King ME, Ménache MG, Miller FJ. Ozone uptake in awake Sprague-Dawley rats. Toxicol Appl Pharmacol 1987;89:429–437
40. Wiester MJ, Stevens MA, Menache MG, McKee JL Jr, Gerrity TR. Ozone uptake in healthy adult males during quiet breathing. Fundam Appl Toxicol 1996;29:102–109
41. Hatch GE, Slade R, Harris LP, et al. Ozone dose and effect in humans and rats. A comparison using oxygen-18 labeling and bronchoalveolar lavage. Am J Respir Crit Care Med 1994;150:676–683
42. Pryor WA, Squadrito GL, Friedman M. The cascade mechanism to explain ozone toxicity: the role of lipid ozonation products. Free Radic Biol Med 1995;19:935–941
43. Sathishkumar K, Haque M, Perumal TE, Francis J, Uppu RM. A major ozonation product of cholesterol, 3beta-hydroxy-5-oxo-5,6-secocholestan-6-al, induces apoptosis in H9c2 cardiomyoblasts. FEBS Lett 2005;579:6444–6450
44. Sathishkumar K, Xi X, Martin R, Uppu RM. Cholesterol secoaldehyde, an ozonation product of cholesterol, induces amyloid aggregation and apoptosis in murine GT1-7 hypothalamic neurons. J Alzheimers Dis 2007;11:261–274
45. Demozay D, Mas J-C, Rocchi S, Van Obberghen E. FALDH reverses the deleterious action of oxidative stress induced by lipid peroxidation product 4-hydroxynonenal on insulin signaling in 3T3-L1 adipocytes. Diabetes 2008;57:1216–1226
46. Pillon NJ, Vella RE, Souleere L, Becchi M, Lagarde M, Soulage CO. Structural and functional changes in human insulin induced by the lipid peroxidation byproducts 4-hydroxy-2-nonenal and 4-hydroxy-2-hexenal. Chem Res Toxicol 2011;24:752–762
47. Mudway IS, Krishna MT, Frew AJ, et al. Compromised concentrations of ascorbate in fluid lining the respiratory tract in human subjects after exposure to ozone. Occup Environ Med 1999;56:473–481
48. Watterson TL, Hamilton B, Martin R, Coulombe RA Jr. Urban particulate matter causes ER stress and the unfolded protein response in human lung cells. Toxicol Sci 2009;112:111–122
49. Ozcan U, Cao Q, Yilmaz E, et al. Endoplasmic reticulum stress links obesity, insulin action, and type 2 diabetes. Science 2004;306:457–461
50. Ozcan U, Yilmaz E, Ozcan L, et al. Chemical chaperones reduce ER stress and restore glucose homeostasis in a mouse model of type 2 diabetes. Science 2006;313:1137–1140
51. Tanti J-F, Jager J. Cellular mechanisms of insulin resistance: role of stress-regulated serine kinases and insulin receptor substrates (IRS) serine phosphorylation. Curr Opin Pharmacol 2009;9:753–762
52. Zheng Z, Xu X, Zhang X, et al. Exposure to ambient particulate matter induces a NASH-like phenotype and impairs hepatic glucose metabolism in an animal model. J Hepatol 2013;58:148–154
53. Henstridge DC, Bruce CR, Pang CP, et al. Skeletal muscle-specific overproduction of constitutively activated c-Jun N-terminal kinase (JNK) induces insulin resistance in mice. Diabetologia 2012;55:2769–2778